Energy-based Modeling of Tangential Compliance in 3-Dimensional Impact

Yan-Bin Jia[1]

Department of Computer Science, Iowa State University, jia@cs.iastate.edu

Abstract. This paper studies modeling of tangential compliance as two rigid bodies collide in the space. Stronge's spring-based contact structure [13, pp. 95-96] is extended to three dimensions. Slip or stick is indicated by the tangential motion of a massless particle connected to the contact point (viewed as an infinitesimal region) on one body via three orthogonal springs. We show that the effect of tangential compliance can be analyzed using normal impulse rather than time, contrary to a previous claim by Stronge. This is primarily due to the ability of updating the elastic energies of the three springs without knowledge of their stiffnesses or length changes. The change rates, nevertheless, are computable. So are sliding velocity and tangential impulse. The latter is then integrated into impact equations and contact kinematics, making the whole system driven by normal impulse alone. Examples include a ball and a pencil bouncing on a table, and a massé billiard shot. The theory has potential impact on impulsive robotic manipulation in which the ability to deal with friction and compliance is vital for skillful maneuvers.

1 Introduction

Impulse-based manipulation is an area in robotics where very little work [6,14] is known. An impulsive force has very short execution time, and thus good potential for improving task efficiency. Its use could considerably simplify the robotic mechanism needed to perform a manipulation task, while avoiding uncertainties accumulated over repeated complex operations. The primary reason for the lack of research attention is possibly because the foundation of modeling rigid body impact is not fully developed and the existing theories often seem either too simple to be realistic or too complex to be applicable, especially in the presence of friction and compliance, not to mention nonlinear viscoelastic effects. Discrepancies often exist between an introduced theory and the findings from an experiment intended for its validation.

Before presenting some related work on impact mechanics, we give a brief review of rigid body impact. Suppose during an impact the ith contact force $\boldsymbol{f}_i$ is applied at the location $\boldsymbol{r}_i$ on a body. Integration of the acceleration equation $\dot{\boldsymbol{V}} = d\boldsymbol{V}/dt = \sum_i \boldsymbol{f}_i/m$ over the impact duration Δt yields the total impulse $\sum_i \boldsymbol{I}_i = m\Delta\boldsymbol{V}$. Similarly, integrating the angular acceleration equation $\sum_i \boldsymbol{r}_i \times \boldsymbol{f}_i = Q\dot{\boldsymbol{\omega}} + \boldsymbol{\omega} \times Q\boldsymbol{\omega}$, where Q is the body's angular inertia matrix, we obtain $\sum_i \boldsymbol{r}_i \times \boldsymbol{I}_i = Q\Delta\boldsymbol{\omega}$ since $\boldsymbol{\omega}$ is bounded and $\Delta t \to 0$. The

following linear impact equations relate the body's velocities to individual impulses:

$$\Delta V = \frac{1}{m}\sum_i \boldsymbol{I}_i \quad \text{and} \quad \Delta\boldsymbol{\omega} = Q^{-1}\sum_i (\boldsymbol{r}_i \times \boldsymbol{I}_i). \tag{1}$$

An impulse $\boldsymbol{I}$ can be decomposed into a component of magnitude I_n along the contact normal and a tangential component $\boldsymbol{I}_\perp$. The normal impulse I_n increases during both compression and restitution phases of impact. The ratio of its amount of accumulation during restitution to that during compression is a constant under Poisson's hypothesis. In solving an impact problem, I_n is often treated as the variable [9] with whose growth the velocities, the contact mode, and the impact phase are updated.

The tangential impulse $\boldsymbol{I}_\perp$, meanwhile, depends on the sequence of contact modes that occur during the impact. If the contact is sliding, the differential accumulations $d\boldsymbol{I}_\perp$ and dI_n are related under Coulomb's law of friction, with the former opposing the instantaneous slip direction. If the contact is sticking, $d\boldsymbol{I}_\perp$ is in a direction to counter the tendency of slip. As the direction varies, the tangential impulse accumulates along a plane curve, and the total impulse along a space curve. A closed-form solution rarely exists.

Efforts on impact analysis have struggled over the consistencies between laws of Coulomb's friction and energy conservation, and Poisson's impulse-based hypothesis of restitution. Routh's graphical method [10] to construct the impulse trajectory has proven successful for analyzing 2-dimensional impacts, and has been later extended by various researchers [4,15,1]. For 3-dimensional impact, Darboux [3] was the first to describe impact dynamics in terms of normal impulse in the form of a differential equation. His result was later rediscovered by Keller [9] who also used the equation's solution to determine the varying slip direction.

The above efforts have neglected the effect of tangential compliance and assumed that all work done by the tangential reaction force is lost to friction. When tangential compliance is not negligible, however, part of the work is converted into recoverable internal energy, despite the loss of the remaining part to friction. The approaches [2,11], designed to produce a ratio of tangential to normal impulse equal to the coefficient of friction, did not exactly follow Coulomb's law of friction. Stronge [13] developed a lumped parameter representation of compliance, and applied a time-dependent analysis to track the change in the tangential velocity during a collision. His model could predict slip or stick at the contact under Coulomb's law. However, without knowing the duration of impact, the analysis can only be used to perceive contact modes qualitatively rather than to carry out specific computation.

Computation of tangential impulse is the key to solving an impact problem and the focus of this paper. We extend the structure of Stronge's linear model of planar impact with compliance [13, pp. 95-96] to develop a theory for 3-dimensional impact that is based on normal impulse only and consistent with both laws of Coulomb friction and energy conservation.

2 Tangential Impulse

During a collision of two bodies, the gravitational forces are negligible compared to the contact force. The configuration can be oriented to keep the contact tangent plane horizontal. To model tangential compliance, we first extend the planar contact structure used by Stronge [13, pp. 95–96] to three dimensions. The "contact point" on the upper body does not directly touch the lower body but is rather connected to a massless particle p via three springs respectively aligned with the upward normal $\hat{\boldsymbol{n}}$ and two orthogonal tangential directions $\hat{\boldsymbol{u}}$ and $\hat{\boldsymbol{w}}$, all unit vectors, as shown in Fig. 1. The di-

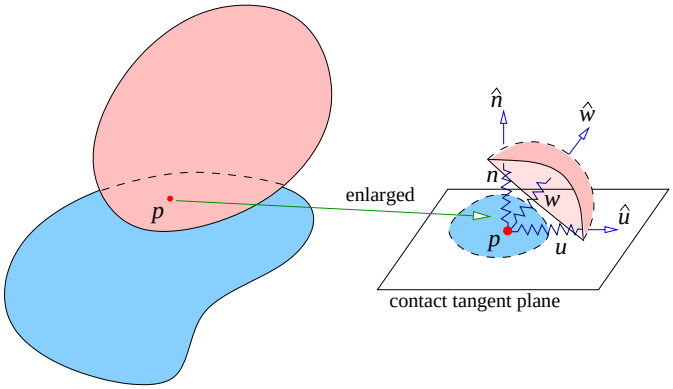

Fig. 1. Compliance model for 3-dimensional impact. The contact point, initially coinciding with the particle p, is blown up into a small region (shown on the right) connected to p via three springs.

rection $\hat{\boldsymbol{u}}$ is chosen to oppose the tangential component of the initial contact velocity $\boldsymbol{v}_0$, and $\hat{\boldsymbol{w}} = \hat{\boldsymbol{n}} \times \hat{\boldsymbol{u}}$. All velocities will be measured along these directions but not relative to p which may move during impact.

The contact force $\boldsymbol{F}$ on the upper body is decomposed as $\boldsymbol{F} = F_u\hat{\boldsymbol{u}} + F_w\hat{\boldsymbol{w}} + F_n\hat{\boldsymbol{n}}$, with each component exerted by one of the three springs. The impulse $\boldsymbol{I} = \int \boldsymbol{F}\, dt$ also has components I_n, I_u, I_w, respectively in the three orthogonal directions; namely,

$$\boldsymbol{I} = I_n\hat{\boldsymbol{n}} + I_u\hat{\boldsymbol{u}} + I_w\hat{\boldsymbol{w}}. \tag{2}$$

2.1 Impact Model

The impact starts with compression and ends with restitution. In the compression phase, the normal spring compresses and its elastic energy E_n builds up while the normal component v_n of the contact velocity $\boldsymbol{v}$ decreases. Compression ends when $v_n = 0$; at this moment E_n has the maximum value, say, $E_{\max}$. During restitution, the normal spring extends, releasing an amount $e^2E_{\max}$

of the energy, where $e \in [0,1]$ is referred to as the *energetic coefficient of restitution*. The conventional kinetic coefficient of restitution, introduced by Poisson as the ratio between the normal impulse released during restitution to that accumulated during compression, is not consistent with energy conservation when the direction of contact slip varies during collision [13, p. 47].

We adopt Stronge's explanation [13, p. 96] for the energy loss $(1-e^2)E_{\max}$: at the moment restitution starts, the normal stiffness suddenly scales up $1/e^2$ times. Namely, the normal stiffness k during the impact is given by

$$k = \begin{cases} k_0, & \text{compression,} \\ k_0/e^2, & \text{restitution.} \end{cases} \tag{3}$$

where k_0 is the original stiffness. Meanwhile, the change n in the normal spring length suddenly varies by a factor of e^2. The normal contact force F_n nevertheless stays the same at this phase transition.

The two tangential springs have the same stiffness $k_\perp$ which is invariant during the impact. The ratio $\eta_0^2 = k_0/k_\perp$ is often considered a constant that depends on the Young's moduli and the Poisson's ratios of the materials in contact.[1] In the analysis below, we will use the ratio

$$\eta^2 = k/k_\perp, \tag{4}$$

where $\eta = \eta_0$ during compression and $\eta = \eta_0/e$ during restitution.

Denote by n, u, w the *changes of length* of the three springs, and E_n, E_u, E_w the elastic energies they store, respectively. The contact force components and the elastic energies are given below:

$$F_n = -kn \geq 0, \quad F_u = -k_\perp u, \quad F_w = -k_\perp w; \tag{5}$$

$$E_n = \frac{1}{2}kn^2, \qquad E_u = \frac{1}{2}k_\perp u^2, \quad E_w = \frac{1}{2}k_\perp w^2. \tag{6}$$

Impulse Derivatives Our objective is to describe the entire system in terms of the normal impulse I_n. To avoid any ambiguity, from now on the notation '˙' will refer to differentiation with respect to time, while the notation '′' will refer to differentiation with respect to I_n (which monotonically increases from zero during impact).

Combining the first equations in (5) and (6), the change rate of the normal impulse I_n over time can be described in terms of the elastic energy E_n:

$$\dot{I}_n = dI_n/dt = F_n = \sqrt{2kE_n}. \tag{7}$$

The derivative is well-defined at the impact phase transition where F_n stays continuous. Meanwhile, from $\dot{n} = v_n$, the normal contact velocity, and $\dot{I}_n = F_n = -kn$ we obtain that $\dot{E}_n = kn\dot{n} = -v_n\dot{I}_n$, thereby the derivative

$$E_n' = dE_n/dI_n = \dot{E}_n/\dot{I}_n = -v_n. \tag{8}$$

[1] For normal indentation by a rigid circular punch on an elastic half space, Johnson [8, pp. 361–366] showed that $\eta_0^2 = \frac{2-\nu}{2(1-\nu)}$, where ν is the Poisson's ratio of the half space. For most materials, this ratio ranges between 0 and 0.5 (Wikipedia).

Similarly, from the other two pairs of equations in (5) and (6) we obtain the change rates of the two tangential impulses:

$$\dot{I}_u = F_u = -\alpha\sqrt{2k_\perp E_u} \quad \text{and} \quad \dot{I}_w = F_w = -\beta\sqrt{2k_\perp E_w}, \tag{9}$$

where α and β are the signs of the length changes of the u- and w-springs, i.e.,

$$\alpha = \begin{cases} 1 \text{ if } u \geq 0, \\ -1 \text{ if } u < 0; \end{cases} \qquad \beta = \begin{cases} 1 \text{ if } w \geq 0, \\ -1 \text{ if } w < 0. \end{cases} \tag{10}$$

Equation (7) is important because it allows us to convert a derivative with respect to time into one with respect to the normal impulse I_n simply by a division over $\sqrt{2kE_n}$. As an illustration, we have

$$I'_u = \frac{\dot{I}_u}{\dot{I}_n} = -\alpha\sqrt{\frac{k_\perp E_u}{kE_n}} = -\frac{\alpha}{\eta}\sqrt{\frac{E_u}{E_n}} \quad \text{and} \quad I'_w = -\frac{\beta}{\eta}\sqrt{\frac{E_w}{E_n}}. \tag{11}$$

In fact, the stiffnesses k and $k_\perp$ will always occur together in the ratio form.

2.2 Contact Modes

The contact velocity $\boldsymbol{v}$ of the two bodies is obtained from their velocities and angular velocities as well as the locations of contact on each body, based on the contact kinematics. This will be illustrated in the examples in Section 3. For now we just assume that $\boldsymbol{v}$ is provided, and denote its tangential component as $\boldsymbol{v}_\perp$. Then the velocity of the particle p is

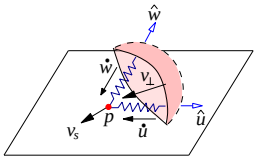

Fig. 2. Sliding velocity of the contact particle p.

$$\boldsymbol{v}_s = \boldsymbol{v}_\perp - \dot{u}\hat{\boldsymbol{u}} - \dot{w}\hat{\boldsymbol{w}}. \tag{12}$$

When $\boldsymbol{v}_s = 0$, i.e., $\boldsymbol{v}_\perp = \dot{u}\hat{\boldsymbol{u}} + \dot{w}\hat{\boldsymbol{w}}$, the contact sticks. In other words, the relative motion of the upper body to the lower body in the contact plane is completely absorbed by the two tangential springs so that p has no motion. When $\boldsymbol{v}_s \neq 0$, it is the *sliding velocity* of the contact.

When slip happens, under Coulomb's law, the tangential contact force $\boldsymbol{F}_\perp = -\mu F_n \hat{\boldsymbol{v}}_s$, where μ is the friction coefficient[2] and

$$\hat{\boldsymbol{v}}_s = \frac{\boldsymbol{v}_s}{\|\boldsymbol{v}_s\|} = \frac{\boldsymbol{v}_\perp - \dot{u}\hat{\boldsymbol{u}} - \dot{w}\hat{\boldsymbol{w}}}{\|\boldsymbol{v}_s\|}, \qquad \text{from (12)}. \tag{13}$$

Since the force also exerts on the u- and w-springs, we obtain

$$k_\perp(u\hat{\boldsymbol{u}} + w\hat{\boldsymbol{w}}) = \mu F_n \hat{\boldsymbol{v}}_s, \tag{14}$$

[2] The difference between static and dynamic coefficients is ignored so the value of μ stays constant whether the contact sticks or slips.

Substitute (13) into (14), and rearrange the terms slightly:

$$\boldsymbol{v}_\perp - \dot{u}\hat{\boldsymbol{u}} - \dot{w}\hat{\boldsymbol{w}} = \frac{k_\perp}{\mu F_n}\|\boldsymbol{v}_s\|(u\hat{\boldsymbol{u}} + w\hat{\boldsymbol{w}}). \tag{15}$$

Equation (15) also holds under the sticking contact since it reduces to $\boldsymbol{v}_\perp = \dot{u}\hat{\boldsymbol{u}} + \dot{w}\hat{\boldsymbol{w}}$ when $\boldsymbol{v}_s = 0$. Take dot products of both sides of (15) with $\hat{\boldsymbol{u}}$, and then multiply by w. Similarly, take dot products with $\hat{\boldsymbol{w}}$ and multiply by u. Subtracting the two resulting equations, we have, under both contact modes,

$$w\dot{u} - u\dot{w} = (\boldsymbol{v}_\perp \cdot \hat{\boldsymbol{u}})w - (\boldsymbol{v}_\perp \cdot \hat{\boldsymbol{w}})u. \tag{16}$$

The contact between the two bodies sticks when $\sqrt{F_u^2 + F_w^2} < \mu F_n$, namely, by (9), when

$$\sqrt{\dot{I}_u^2 + \dot{I}_w^2} < \mu \dot{I}_n. \tag{17}$$

To replace the time derivatives, we substitute equations (7) and (9) into the above, and rearrange the resulting terms after squaring both sides:

$$E_u + E_w < \mu^2\eta^2 E_n. \tag{18}$$

When the contact slips, we have the equality

$$E_u + E_w = \mu^2\eta^2 E_n. \tag{19}$$

2.3 Stick

Since $\boldsymbol{v}_s = 0$, the lengths of the u- and w-springs change at rates

$$\dot{u} = \boldsymbol{v}_\perp \cdot \hat{\boldsymbol{u}} = \boldsymbol{v} \cdot \hat{\boldsymbol{u}} \quad \text{and} \quad \dot{w} = \boldsymbol{v} \cdot \hat{\boldsymbol{w}}. \tag{20}$$

Their length changes are

$$u = \int \dot{u}\, dt = \int \frac{\dot{u}}{\dot{I}_n}\, dI_n = \int \frac{\dot{u}}{\sqrt{2kE_n}}\, dI_n = \frac{1}{\sqrt{2k}} \int \frac{\boldsymbol{v}_\perp}{\sqrt{E_n}}\, dI_n \cdot \hat{\boldsymbol{u}},$$
$$w = \frac{1}{\sqrt{2k}} \int \frac{\boldsymbol{v}_\perp}{\sqrt{E_n}}\, dI_n \cdot \hat{\boldsymbol{w}}.$$

Suppose compression ends at $I_n = I_c$ and restitution ends at $I_n = I_r$. Observing (3), we introduce a vector integral

$$\boldsymbol{D} = \begin{cases} \int_0^{I_n} \frac{\boldsymbol{v}_\perp}{\sqrt{E_n}}\, dI_n, & \text{if } I_n \in [0, I_c); \\ \int_0^{I_c} \frac{\boldsymbol{v}_\perp}{\sqrt{E_n}}\, dI_n + \int_{I_c}^{I_n} e\frac{\boldsymbol{v}_\perp}{\sqrt{E_n}}\, dI_n, & \text{if } I_n \in [I_c, I_r], \end{cases} \tag{21}$$

so that during impact the following always hold:

$$u = \frac{\boldsymbol{D} \cdot \hat{\boldsymbol{u}}}{\sqrt{2k_0}} \quad \text{and} \quad w = \frac{\boldsymbol{D} \cdot \hat{\boldsymbol{w}}}{\sqrt{2k_0}}. \tag{22}$$

Instead of computing u and w, we keep track of $\sqrt{2k_0}u$ and $\sqrt{2k_0}w$ by updating $\boldsymbol{D}$, without any knowledge about k_0.

The update of $\boldsymbol{D}$ is possible because $\boldsymbol{v}_\perp$ is from the contact kinematics, and E_n is by (6). The values of α and β in (10) are immediately known from the signs of $\boldsymbol{D}\cdot\hat{\boldsymbol{u}}$ and $\boldsymbol{D}\cdot\hat{\boldsymbol{w}}$. The integral is also used to conveniently evaluate the tangential elastic energies, for

$$E_u = \frac{1}{2}k_\perp u^2 \;=\; \frac{1}{4}\frac{k_\perp}{k_0}(\boldsymbol{D}\cdot\hat{\boldsymbol{u}})^2 = \frac{1}{4\eta_0^2}(\boldsymbol{D}\cdot\hat{\boldsymbol{u}})^2 \;\text{ and }\; E_w = \frac{1}{4\eta_0^2}(\boldsymbol{D}\cdot\hat{\boldsymbol{w}})^2. \tag{23}$$

2.4 Slip

When the contact slips, equation (19) holds. We substitute the spring energies E_u and E_w from (6) in and obtain, by the use of (4),

$$u^2 + w^2 = 2\mu^2\frac{k}{k_\perp^2}E_n. \tag{24}$$

Then differentiate (24) with respect to time:

$$u\dot{u} + w\dot{w} = \mu^2\frac{k}{k_\perp^2}\dot{E}_n. \tag{25}$$

Now, we can solve the spring velocities $\dot{u}$ and $\dot{w}$ from (16) and (25):

$$\dot{u} = \frac{\alpha\mu^2\eta^3E_n'\sqrt{E_nE_u} + (\boldsymbol{v}_\perp\cdot\hat{\boldsymbol{u}})E_w - \alpha\beta(\boldsymbol{v}_\perp\cdot\hat{\boldsymbol{w}})\sqrt{E_uE_w}}{\mu^2\eta^2E_n}, \tag{26}$$

$$\dot{w} = \frac{\beta\mu^2\eta^3E_n'\sqrt{E_nE_w} + (\boldsymbol{v}_\perp\cdot\hat{\boldsymbol{w}})E_u - \alpha\beta(\boldsymbol{v}_\perp\cdot\hat{\boldsymbol{u}})\sqrt{E_uE_w}}{\mu^2\eta^2E_n}. \tag{27}$$

With $\dot{u}$ and $\dot{w}$ known, the sliding velocity $\boldsymbol{v}_s$ follows from (12).

The change rates (26) and (27) do not tell whether the springs are being compressed (e.g., $u<0$) or elongated (e.g., $u>0$). Since

$$u = \int\dot{u}\,dt = \int\frac{\dot{u}}{\sqrt{2kE_n}}\,dI_n \quad\text{and}\quad w = \int\frac{\dot{w}}{\sqrt{2kE_n}}\,dI_n, \tag{28}$$

we introduce two integrals G_u and G_w, where for $\rho = u, v$,

$$G_\rho = \begin{cases} \int_0^{I_n}\frac{\dot{\rho}}{\sqrt{E_n}}\,dI_n, & \text{if } I_n\in[0,I_c), \\ \int_0^{I_c}\frac{\dot{\rho}}{\sqrt{E_n}}\,dI_n + \int_{I_c}^{I_n}e\frac{\dot{\rho}}{\sqrt{E_n}}\,dI_n, & \text{if } I_n\in[I_c,I_r]; \end{cases} \tag{29}$$

Comparing these two equations with (28), $G_u = \sqrt{2k_0}u$ and $G_w = \sqrt{2k_0}w$.

The two integrals G_u and G_w are used to not only track the signs of u and w but also update tangential elastic energies as follows:

$$E_u = \frac{1}{2}k_\perp u^2 = \frac{G_u^2}{4\eta_0^2} \quad\text{and}\quad E_w = \frac{G_w^2}{4\eta_0^2}. \tag{30}$$

2.5 Contact Mode Transitions

At a contact mode switch, we need to initialize the integrals $\boldsymbol{D}$ or G_u and G_w in order to track whether the tangential springs are being compressed or extended and update E_u and E_w during the next contact mode.

Stick to Slip The contact point switches its mode when $F_u^2 + F_w^2 = \mu^2 F_n^2$, i.e., when (19) holds. We initialize the integrals for slip using (30):

$$G_u = 2\alpha\eta_0\sqrt{E_u} \quad \text{and} \quad G_w = 2\beta\eta_0\sqrt{E_w}, \tag{31}$$

where E_u, E_w, α and β inherit their values from just before the change of contact.

Slip to Stick The contact switches from slip to stick when the sliding velocity $\boldsymbol{v}_s$ vanishes, that is, when

$$\boldsymbol{v}_\perp = \dot{u}\hat{\boldsymbol{u}} + \dot{w}\hat{\boldsymbol{w}} \tag{32}$$

from (12). Equations (22) imply that

$$\begin{aligned}\boldsymbol{D} = \sqrt{2k_0}(u\hat{\boldsymbol{u}} + w\hat{\boldsymbol{u}}) \;&=\; \sqrt{2k_0}\left(\alpha\sqrt{\frac{2E_u}{k_\perp}}\hat{\boldsymbol{u}} + \beta\sqrt{\frac{2E_w}{k_\perp}}\hat{\boldsymbol{w}}\right) \quad \text{by (6) and (10)} \\ &= 2\eta_0\left(\alpha\sqrt{E_u}\hat{\boldsymbol{u}} + \beta\sqrt{E_w}\hat{\boldsymbol{w}}\right). \end{aligned} \tag{33}$$

2.6 Impact Algorithm

The system of impact equations does not have a closed-form solution in general. Simulation is carried out via numerical integration over I_n with some step size, say, h. The pseudo-code is given below.

```
1  initialization
2  dI_n ← h
3  while (compression or E_n > 0) do
4    if v · n̂ = 0
5      then compression ends
6    if contact sticks
7      then update D according to (21) and E_u, E_w 8 according to (23)
9           if slip starts by (19)
10            then initialize G_u and G_w as (31)
11     else  evaluate u̇, v̇ according to (26), (27)
12           update G_u, G_w according to (29) and E_u, E_w according to (30)
13           if stick starts by (32)
14             then initialize D as (33)
15   evaluate I'_u and I'_w as (11)
16   I ← I + dI_n · (I'_u û + I'_w ŵ + n̂)
17   update V and ω using impact equations (1)
18   update v using V and ω according to contact kinematics
19   E_n ← E_n − v_n dI_n by (8)
```

2.7 Impact Initialization

To start the algorithm, we need to initialize the contact mode, the normal and tangential elastic energies, the integral $\boldsymbol{D}$ or G_u, G_w, accordingly, and the tangential impact. Let the initial contact velocity be $\boldsymbol{v}_0 = v_{0n}\hat{\boldsymbol{n}} + \boldsymbol{v}_{0\perp}$. By (8) we have that $E_n'(0) = -v_{0n}$ and $E_n(h) \approx -v_{0n}h$.

Stick or Slip? We first assume that the impact starts with stick, and apply our analysis from Section 2.3 to derive a condition on $\boldsymbol{v}_0$. Here we look at a small period of time Δt after the impact begins. The force on the u-spring is

$$\dot{I}_u = -k_\perp u = -k_\perp \int_0^{\Delta t} \dot{u}\, dt = -k_\perp \int_0^{\Delta t} (\boldsymbol{v}\cdot\hat{\boldsymbol{u}})\, dt, \quad \text{by (20)}. \tag{34}$$

Similarly, we obtain the forces exerted by the other two springs:

$$\dot{I}_w = -k_\perp \int_0^{\Delta t} (\boldsymbol{v}\cdot\hat{\boldsymbol{w}})\, dt \quad \text{and} \quad \dot{I}_n = -k_0 \int_0^{\Delta t} (\boldsymbol{v}\cdot\hat{\boldsymbol{n}})\, dt. \tag{35}$$

Substitute the above three time derivatives into the sticking contact condition (17) and move the integral over $(\boldsymbol{v}\cdot\hat{\boldsymbol{n}})$ to the left side of the resulting inequality:

$$\begin{aligned}\lim_{\Delta t\to 0} \frac{\|\int_0^{\Delta t}(\boldsymbol{v}\cdot\hat{\boldsymbol{u}})\hat{\boldsymbol{u}} + (\boldsymbol{v}\cdot\hat{\boldsymbol{w}})\hat{\boldsymbol{w}}\, dt\|}{-\int_0^{\Delta t}(\boldsymbol{v}\cdot\hat{\boldsymbol{n}})\, dt} &= \lim_{\Delta t\to 0} \frac{\int_0^{\Delta t}\sqrt{(\boldsymbol{v}\cdot\hat{\boldsymbol{u}})^2 + (\boldsymbol{v}\cdot\hat{\boldsymbol{w}})^2}\, dt}{-\int_0^{\Delta t}(\boldsymbol{v}\cdot\hat{\boldsymbol{n}})\, dt} \\ &= \frac{\sqrt{(\boldsymbol{v}_0\cdot\hat{\boldsymbol{u}})^2 + (\boldsymbol{v}_0\cdot\hat{\boldsymbol{w}})^2}}{-(\boldsymbol{v}_0\cdot\hat{\boldsymbol{n}})} < \mu\frac{k_0}{k_\perp} = \mu\eta_0^2.\end{aligned}$$

The first equation above follows from that $\boldsymbol{v}\cdot\hat{\boldsymbol{u}}$ and $\boldsymbol{v}\cdot\hat{\boldsymbol{w}}$ do not changes signs within Δt. Hence we infer that the impact starts with a sticking contact if

$$(\boldsymbol{v}_0\cdot\hat{\boldsymbol{u}})^2 + (\boldsymbol{v}_0\cdot\hat{\boldsymbol{w}})^2 < \mu^2\eta_0^4(\boldsymbol{v}_0\cdot\hat{\boldsymbol{n}})^2, \tag{36}$$

or a sliding contact if

$$(\boldsymbol{v}_0\cdot\hat{\boldsymbol{u}})^2 + (\boldsymbol{v}_0\cdot\hat{\boldsymbol{w}})^2 \geq \mu^2\eta_0^4(\boldsymbol{v}_0\cdot\hat{\boldsymbol{n}})^2. \tag{37}$$

Initial Stick Using a similar approach, we can obtain the initial values of the derivatives of the tangential impulses when the contact sticks at the beginning:

$$I_u'(0) = \frac{1}{\eta_0^2}\cdot\frac{\boldsymbol{v}_0\cdot\hat{\boldsymbol{u}}}{\boldsymbol{v}_0\cdot\hat{\boldsymbol{n}}} \quad \text{and} \quad I_w'(0) = \frac{1}{\eta_0^2}\cdot\frac{\boldsymbol{v}_0\cdot\hat{\boldsymbol{w}}}{\boldsymbol{v}_0\cdot\hat{\boldsymbol{n}}} = 0. \tag{38}$$

Here, note that the axis $\hat{\boldsymbol{w}}$ is chosen to be perpendicular to $\boldsymbol{v}_{0\perp}$. Next, we substitute $E_n'(I_n) \approx -v_{0n}$ into the integral (21) over $[0, h]$:

$$\begin{aligned}\boldsymbol{D}(h) &= \int_0^h \frac{1}{\sqrt{-v_{0n}I_n + O(I_n^2)}}\, dI_n\cdot\boldsymbol{v}_{0\perp} \approx -\frac{1}{v_{0n}}\cdot 2\sqrt{-v_{0n}I_n}\,\Big|_0^h \cdot\boldsymbol{v}_{0\perp} \\ &= -2\sqrt{-\frac{h}{v_{0n}}}\cdot\boldsymbol{v}_{0\perp}, \quad \text{since } v_{0n} < 0.\end{aligned}$$

The initial elastic energies $E_u(h)$ and $E_w(h)$ of the tangential springs are then evaluated according to (23).

Initial Slip When the contact initially slips, the impulse derivatives follow Coulomb's law; namely,

$$I'_u(0) = -\mu \frac{\boldsymbol{v}_{0\perp} \cdot \hat{\boldsymbol{u}}}{\|\boldsymbol{v}_{0\perp}\|} = \mu \quad \text{and} \quad I'_w(0) = -\mu \frac{\boldsymbol{v}_{0\perp} \cdot \hat{\boldsymbol{w}}}{\|\boldsymbol{v}_{0\perp\|}} = 0, \tag{39}$$

since $\hat{\boldsymbol{u}}$ opposes $\boldsymbol{v}_{0\perp}$ when $\boldsymbol{v}_{0\perp} \neq 0$. The sliding velocity $\boldsymbol{v}_s$ must have the same direction as the direction $\hat{\boldsymbol{t}}$ of the relative tangential velocity $\boldsymbol{v}_{0\perp}$. Substituting (7) into (14) for F_n, we write down the changes of length of the u- and w-springs, and obtain E_u and E_w from (6), and G_u and G_w from (30).

3 Examples of Bouncing

This section demonstrates incorporation of tangential impulse into impact equations (1) using two examples. We look at bounces of a ball and a pencil, which result in planar and space impulse curves, respectively.

3.1 Ball

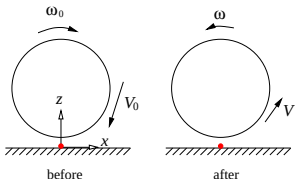

Fig. 3. Bouncing ball.

As shown in Fig. 3, a ball at initial velocity $\boldsymbol{V}_0$ and angular velocity $\boldsymbol{\omega}_0$ collides with a still table. Let r be the ball's radius and m its mass. Hence its angular inertia $\frac{2}{5}mr^2$. Denote by $\hat{\boldsymbol{z}}$ the upward contact normal, and $\boldsymbol{I}$ the impulse exerted by the table on the ball during the collision. The velocity equations (1) specialize to

$$\boldsymbol{V} = \boldsymbol{V}_0 + \frac{\boldsymbol{I}}{m} \quad \text{and} \quad \boldsymbol{\omega} = \boldsymbol{\omega}_0 - \frac{5}{2mr} \hat{\boldsymbol{z}} \times \boldsymbol{I}.$$

We obtain the contact velocity and its tangential component:

$$\boldsymbol{v} = \boldsymbol{V} + \omega \times (-r\hat{\boldsymbol{z}}) = \boldsymbol{v}_0 + \frac{I_z}{m}\hat{\boldsymbol{z}} + \frac{7}{2m}\boldsymbol{I}_\perp,$$

$$\boldsymbol{v}_\perp = \boldsymbol{v}_{0\perp} + \frac{7}{2m}\boldsymbol{I}_\perp,$$

where $\boldsymbol{v}_0$ and $\boldsymbol{v}_{0\perp}$ are their initial values, and $\boldsymbol{I} = I_z\hat{\boldsymbol{z}} + \boldsymbol{I}_\perp$. We also obtain $E'_z = \frac{dE_z}{dI_z} = -(\hat{\boldsymbol{z}} \cdot \boldsymbol{v}_0) - \frac{I_z}{m}$.

Theorem 1. *During the collision of a ball with a still table, the tangential impulse $\boldsymbol{I}_\perp$ is collinear with the initial tangential contact velocity $\boldsymbol{v}_{0\perp}$.*

The proof is by induction over the number of contact mode transitions. Details are omitted due to lack of space.

Impulse Curve Theorem 1 states that the impulse curve $\boldsymbol{I}$ lies in the vertical plane spanned by the z-axis and $\boldsymbol{v}_{0\perp}$.[3] So we can conveniently place the origin at the contact point, and the x-axis in the opposite direction of $\boldsymbol{v}_{0\perp}$. The x-y-z frame is identified with the n-u-w contact frame for tangential impulse in Section 2.

For simplicity, consider $m = 1$ and $r = 1$. Let the coefficient of friction be $\mu = 0.4$, the coefficient of restitution $e = 0.5$, and Poisson's ratio of the ball $\nu = 0.3$. Here, we use $\eta_0^2 = (2-\nu)/(2-2\nu)$ for a circular punch on a half space [8, pp. 361–366]. Consider $\boldsymbol{V}_0 = (-1, 0, -5)$ and $\boldsymbol{\omega}_0 = (0, 2, 0)$, which yields $\boldsymbol{V}_{0\perp} = (-3, 0, 0)$. After the collision, the ball will bounce backward with a reversal of its rotation: $\boldsymbol{V} = (V_x, 0, V_z) = (0.570982, 0, 2.5)$ and $\boldsymbol{\omega} = (0, \omega_y, 0) = (0, -1.92746, 0)$. Its total energy will decrease from 13.4 to 3.65997.

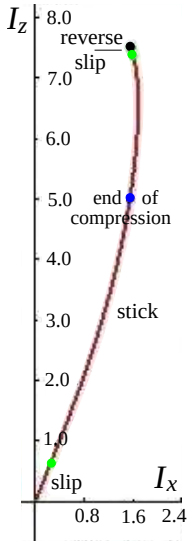

Fig. 4. Impulse curve.

Fig. 4 plots the impulse curve, on which the blue and black dots mark the ends of compression and restitution, respectively, and the two green dots mark the contact mode transitions. The impact starts with a slip, changes from slip to stick at $I_z = 0.62485$, ends compression at $I_z = -mv_{0z} = 5$, starts a reverse slip at $I_z = 7.36575$, and ends restitution at $I_z = -(1+e)mv_{0z} = 7.5$.

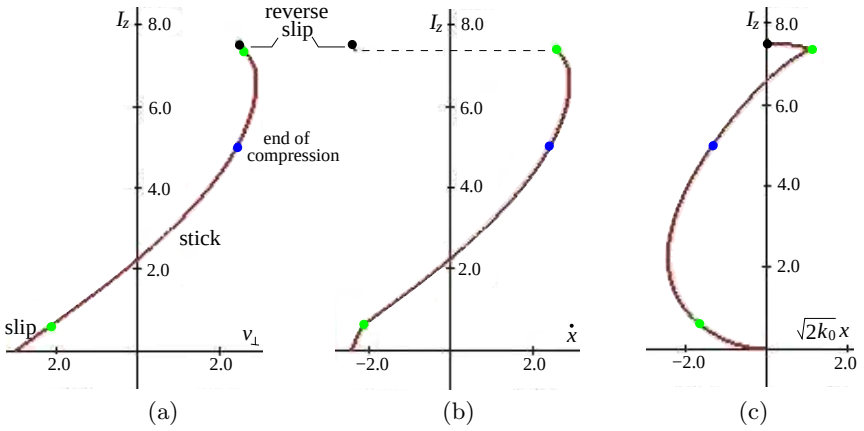

Fig. 5. (a) Tangential contact velocity; (b) x-spring velocity; and (c) varying spring length x scaled by $\sqrt{2k_0}$. The dashed line in (b) marks a discontinuity as reverse slip happens.

[3] It degenerates into a vertical line segment when $\boldsymbol{v}_{0\perp} = 0$.

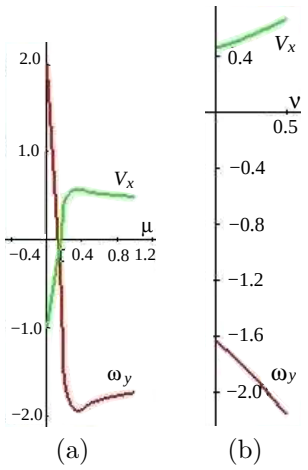

Fig. 6. Effects of (a) friction and (b) Poisson's ratio.

During the impact, the tangential contact velocity and spring velocity, aligned with the x-axis, are treated as scalars here and denoted $v_\perp$ and $\dot{x}$, respectively. As shown in Fig. 5(a), $v_\perp$ starts at -3 and ends at 2.49847. The x-spring velocity increases from -2.42852 with I_z until it equals $v_\perp$ at -2.12528, when the contact switches from slip to stick. Fig. 5(b) shows a sudden change of $\dot{x}$ from 2.59255 to -2.29806 when a slip reversal occurs at $I_z = 7.36575$. To see why, note that under slip $\dot{x}$ must satisfy (25), which becomes $x\dot{x} = (\mu^2 k/k_\perp^2)\dot{E}_z$. Because the transition happens during restitution, $\dot{E}_z < 0$, so x and $\dot{x}$ must have opposite signs at the moment. However, as shown in Fig. 5(b) and (c), both $\dot{x}$ and x were positive before the slip reversal. Hence the sudden change in $\dot{x}$. We can show that during stick the massless particle is in a simple harmonic motion.

Effect of Friction Fig. 6(a) plots the post-impact velocities V_x and ω_y as the coefficient of friction μ varies from 0 to 1.0, where $\boldsymbol{V}_0 = (-1, 0, -5)$ and $\boldsymbol{\omega}_0 = (0, 2, 0)$. When friction is low ($\mu \leq 0.13$), the ball will bounce to the left but keep the original clockwise rotation about the y-axis. As μ increases from 0.13 but does not exceed 0.16, the ball will reverse its rotation but still bounce to the left. As friction becomes higher ($\mu > 0.16$), the ball will bounce backward with a rotation reversal. At $\mu = 0.36$, both v_x and ω_y reach their extrema 0.57591 and -1.93976, respectively.

Effect of Compliance The dependence of V_x and ω_y on Poisson's ratio ν over its normal range $[0, 0.5]$ is shown in Fig. 6(b). Again, $\boldsymbol{V}_0 = (-1, 0, -5)$ and $\boldsymbol{\omega}_0 = (0, 2, 0)$. As ν increases from 0 to 0.5, V_x after the impact increases monotonically from 0.45729 to 0.66507, while ω_y decreases monotonically from -1.64322 to -2.16266. The more compliance, the less energy loss.

3.2 Pencil

We move on to consider another task which many of us may have tried on a

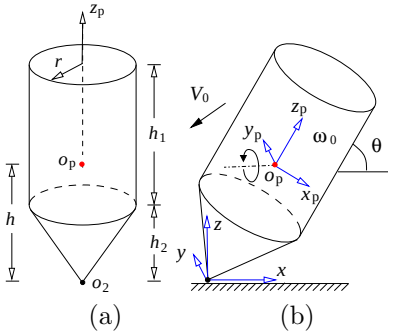

Fig. 7. Pencil with velocities $\boldsymbol{V}_0$ and $\boldsymbol{\omega}_0$ hitting a table: (a) dimensions and (b) frames.

desk — throwing a pencil and watching how it bounces. Most of the time the pencil is thrown with its rubber eraser downward, but here let us consider a pencil strike with the pointed end contacting the desk.

As shown in Fig. 7(a), the pencil is modeled as a cylinder with mass m_1 and height h_1 on top of a cone with mass m_2 and height h_2, where both components have the same mass density. The cross sections of the cylinder and the top face of the cone have the same radius r. The pencil's center of mass o_p is located on its axis of symmetry at distance h above the cone's vertex o_2, where $h = (6h_1^2 + 12h_1h_2 + 3h_2^2)/(12h_1 + 4h_2)$. A body frame x_p-y_p-z_p is placed at o_p with the z_p-axis aligned with the pencil's axis of symmetry.

The moment of inertia Q of the pencil about its center of mass o_p is a diagonal matrix with first two principal moments:

$$Q_{11} = Q_{22} = \frac{m}{h_1 + h_2/3}\left(h_1\Big(\frac{3r^2 + h_1^2}{12} + l^2\Big) + \frac{h_2}{3}\left(\frac{3}{5}\Big(\frac{r^2}{4} + h_2^2\Big) + h^2\right)\right),$$

where $m = m_1 + m_2$ and $l = h_1/2 + h_2 - h$.

The pencil's axis lies in a vertical plane at the moment of the strike. Let this plane be both the x-z plane of the desk frame at the contact point and the x_p-z_p plane of the pencil's body frame. See Fig. 7(b). The pencil, tilted at an angle θ just before the hit, has velocity $\boldsymbol{V}_0$ relative to the desk frame and angular velocity $\boldsymbol{\omega}_0 = (\omega_1, \omega_2, \omega_3)$ relative to a (fixed) frame instantaneously coinciding with the pencil frame. The orientation of the pencil frame in the desk frame is described by a rotation matrix R about the y-axis through θ. The velocities are determined from the impulse $\boldsymbol{I} = (I_x, I_y, I_z)$:

$$\boldsymbol{V} = \boldsymbol{V}_0 + \frac{\boldsymbol{I}}{m} \quad \text{and} \quad -h\hat{\boldsymbol{z}}_\mathrm{p} \times (R^{-1}\boldsymbol{I}) = Q(\boldsymbol{\omega} - \boldsymbol{\omega}_0).$$

The velocity of the contact point during the strike is linear in $\boldsymbol{I}$:

$$\boldsymbol{v} = \boldsymbol{V}_0 + \frac{\boldsymbol{I}}{m} + h\begin{pmatrix} -\omega_2 \sin\theta \\ \omega_1 \\ \omega_2 \cos\theta \end{pmatrix} + \frac{h^2}{Q_{22}}\begin{pmatrix} I_x \sin^2\theta - I_z \sin\theta\cos\theta \\ I_y \\ -I_x \sin\theta\cos\theta + I_z \cos^2\theta \end{pmatrix}. \quad (40)$$

Specifically, we simulate a pencil with $m = 1$, $r = 0.5$, $h_1 = 3$, and $h_2 = 0.5$. Let $\mu = 0.8$ and $e = 0.5$. The pencil tilts at $\theta = \pi/3$, and strikes the desk with velocities $\boldsymbol{V}_0 = 5(-\cos\frac{\pi}{6}, 0, -\sin\frac{\pi}{6})$ and $\boldsymbol{\omega}_0 = (-1, -0.5, -0.5)$. The post-impact velocities are $\boldsymbol{V} = (-0.368092, 0.390783, 3.03015)$ and $\boldsymbol{\omega} = (-0.236153, -1.80209, -0.5)$. The pencil bounces upward with reduced motion along the negative x-direction. It has gained a new motion along the negative y-axis. The angular velocity has changed along both x_p- and y_p-axes in the pencil's body frame. Its component along the z_p axis, i.e., the axis of symmetry, remains as 0.5, due to zero torque about the axis during impact.

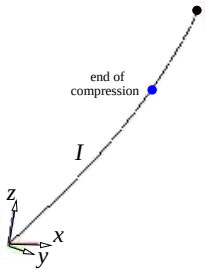

Fig. 8. Impulse curve.

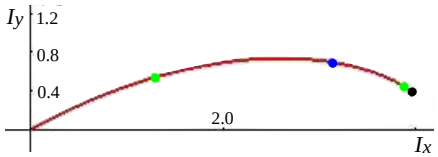

Fig. 9. Tangential impulse.

Fig. 8 plots the impulse curve, which grows from the origin to $(3.96204, 0.390783, 5.53015)$. The contact point slides during impact. The impulse projection onto I_x-I_y plane (see Fig. 9) is also a curve. This shows that the sliding direction was constantly changing in the impact duration.

4 Simultaneous Collisions with Compliance

In [7], we introduced a method to model simultaneous collisions of multiple objects based on transitions between states that characterize different combinations of the objects instantaneously in contact. Tangential impulses due to friction were then treated naively without considering compliance. As a result, the effect of a skillful shot like a massé one could not be modeled based on a measured input.

Tangential impulse due to compliance easily applies to simultaneous impacts. We here illustrate over a massé shot (see Fig. 10). The cue stick hits the ball at a point with outward normal $\hat{\boldsymbol{n}}$, and the ball in turn hits the table with upward normal $\hat{\boldsymbol{z}}$. We set up a local frame at the cue-ball contact with axes $\hat{\boldsymbol{n}}$, $\hat{\boldsymbol{u}}$, and $\hat{\boldsymbol{w}}$, and another frame at the ball-table contact with axes $\hat{\boldsymbol{z}}$, $\hat{\boldsymbol{x}}$, and $\hat{\boldsymbol{y}}$.

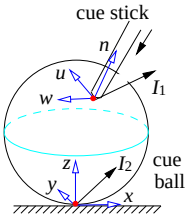

Fig. 10. Billiard shot.

The impulses exerted by the ball on the cue stick and by the table on the ball are respectively $\boldsymbol{I}_1 = I_u\hat{\boldsymbol{u}} + I_w\hat{\boldsymbol{w}} + I_n\hat{\boldsymbol{n}}$ and $\boldsymbol{I}_2 = I_x\hat{\boldsymbol{x}} + I_y\hat{\boldsymbol{y}} + I_z\hat{\boldsymbol{z}}$. According to [7], we can treat exactly one of I_u and I_z as the variable within a state, while the other as a dependent. Now, use the method in Section 2 to obtain I_u and I_w from I_n, and I_x and I_y from I_z. Next, use $\boldsymbol{I}_1$ and $\boldsymbol{I}_2$ to update all velocities, thus closing the loop.

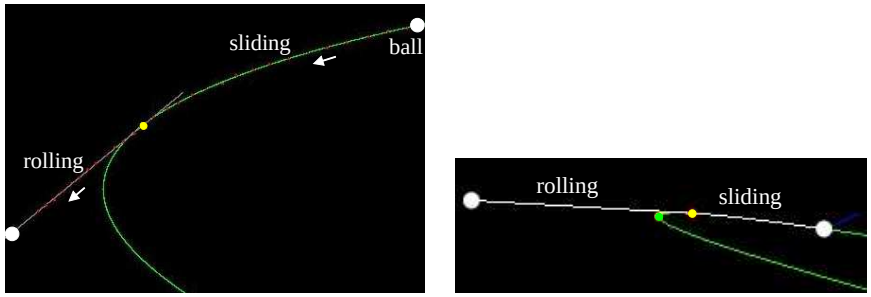

(a) (b)

Fig. 11. Billiard trajectories (a) recovered from the video of a real shot and (b) predicted by the impact model with cue velocity estimated from the same video.

We have designed a mechanical cue stick [7] which allows us to calculate the velocity of the cue tip before a shot. After the shot, the x- and y- components of the ball's velocity and angular velocity can be recovered from its trajectory via some involved steps.

Fig. 11(a) shows the trajectory fit over positions (red dots) sequenced from the video of a shot executed at a point near the top pole of the cue ball. The values of eleven relevant physical constants are omitted due to lack of space. The estimated velocity and angular velocity of the cue ball immediately after the shot are $(-1.65398, -0.36149, \_\_)$ and $(24.2768, 80.537, \_\_)$, respectively.

Fig. 11(b) shows the predicted ball trajectory by the impact model under the same shooting condition. The ball gets velocity $(-1.65774, 0.24380, 0.73265)$ and angular velocity $(15.9378, 52.9882, -3.67556)$. Despite the small differences in the two pairs of velocities, the resulting trajectories differ widely. This is in part due to inaccurate measurements of related physical constants (including a guess over the relative stiffness of the cue-ball and ball-table contacts), the point-based impact model, and uncertainties of the shot.

5 Discussion

The key of the introduced compliance model for impact lies in that the elastic energies stored in the three orthogonal springs can be updated as functions of normal impulse without knowledge about their stiffnesses or length changes. The change rates of the spring lengths are nevertheless computable, so is the sliding velocity. Contact modes are decided from elastic energies rather than forces. All these make computation of tangential impulse possible, with normal impulse the sole variable of the impact problem.

In [13], Stronge claimed that the frictional energy loss depends on the sliding speed (i.e., the particle velocity $\boldsymbol{v}_s$), correcting his earlier statement that it depends on the tangential relative velocity $\boldsymbol{v}$. But it was not until the recent work by Hien [5] was the formulation of frictional dissipation completed. In our work, such dissipation is accounted for as the energies E_u and E_w are stored and released by the two tangential springs.

In their study [16] of a dimer bouncing on a vibrated plate, a similar differential impulse relationship is set up based on the ratio of the potential energies stored at the contact points. Coulomb's friction law is applied over the corresponding impulse increments. In our work, the friction law is applied in the forms (18) and (19) over the elastic energies stored at the contact.

The highly nonlinear nature of impulse accumulation (as shown in the pencil and the billiard examples) due to contact compliance would present an obstacle for formulation of a linear complementarity problem (LCP) as in [12] with a time-stepping solution. Our method is more accurate since it does not approximate the contact friction cone as a polyhedral cone, and also more efficient without having to repetitively solve linear systems.

The next step is to further integrate the compliance model with our previously developed model for simultaneous impacts [7]. Modeling of billiard shots provides a challenging test bed for meshing the two theories. A longer term objective is to apply the theory to impulsive robotic manipulation.

Acknowledgment This work was sponsored in part by Iowa State University. Part of the work was performed in China. The author would like to thank Matt Mason for a pointer to Stronge's work on modeling compliance in impact mechanics, and Mike Erdmann for his encouragement. He is grateful to the anonymous reviewers for their valuable and constructive feedback.

References

1. S. Ahmed, H. M. Lankarani, and M. Pereira. Frictional impact analysis in open-loop multibody mechanical systems. *J. Applied Mech.*, 121:119–126, 1999.
2. R. M. Brach. Tangential restitution in collisions. In L. E. Schwer et al. (ed.), *Computational Techniques for Contact Impact, Penetration and Perforation of Solids*, ASME AMD 103: 1–7, 1989.
3. G. Darboux. Etude géométrique sur les percussions et le choc des corps. *Bulletin des Sciences Mathématiques et Astronomiques, deuxième série, tome 4*, pp. 126–160, 1880.
4. I. Han and B. J. Gilmore. Impact analysis for multiple-body systems with friction and sliding contact. In D. P. Sathyadev (ed.), *Flexible Assembly Systems*, pp. 99-108. American Society Mech. Engineers Design Engr. Div., 1989.
5. T. Hien. A correction on the calculation of frictional dissipation in planar impact of rough compliant bodies by W. J. Stronge. *Int. J. Impact Engr.*, 37:995–998, 2010.
6. W. H. Huang and M. T. Mason. Mechanics, planning, and control for tapping. *Int. J. Robotics*, 19(10):883-894, 2000.
7. Y.-B. Jia, M. Mason, and M. Erdmann. A state transition diagram for simultaneous collisions with application in billiard shooting. In G. Chirikjian, et al. (ed.), *Algorithmic Foundations of Robotics VIII*, pp. 135–150. Springer, 2010.
8. K. L. Johnson. *Contact Mechanics*. Cambridge University Press, 1985.
9. J. B. Keller. Impact with friction. *J. Applied Mech.*, 53(1):1–4, 1986.
10. E. J. Routh. *Dynamics of a System of Rigid Bodies*. MacMillan and Co., 1913.
11. C. E. Smith. Predicting rebounds using rigid-body dynamics. *ASME J. Appl. Mech.*, 58:754–758, 1991.
12. D. E. Stewart and J. C. Trinkle. An implicit time-stepping scheme for rigid body dynamics with inelastic collisions and Coulomb friction. *Int. J. Numer. Methods Engr.*, 39:2673–2691, 1996.
13. W. J. Stronge. *Impact Mechanics*. Cambridge University Press, 2000.
14. K. Tagawa, K. Hirota, and M. Hirose. Manipulation of dynamically deformable object using impulse-based approach. In M. H. Zadeh (ed.), *Advances in Haptics*, pp. 16–33, 2010.
15. Y. Wang and M. T. Mason. Two-dimensional rigid-body collisions with friction. *J. Applied Mech.*, 59:635–642, 1991.
16. Z. Zhao, C. Liu, and B. Brogliato. Planar dynamics of a rigid body system with frictional impacts. *Proc. Royal Soc. A: Math. Phys. Engr. Sci.*, 465:2267–2292, 2009.